The effect of initial conditions on the exit flow from a fluidic precessing jet nozzle

C.Y. Wong, G.J. Nathan, T. O'Doherty

Abstract The fluidic precessing jet (FPJ) is a member of a family of self-excited oscillating jet flows that has found application in reducing oxides of nitrogen (NO_x) from combustion systems in the high-temperature process industries. Its flow field is highly three-dimensional and unsteady, and many aspects of it remain unresolved. Velocity data, measured close to the exit plane, are presented for a variety of FPJ nozzles with three different inlet conditions, namely, a long pipe, a smooth contraction and an orifice. The results indicate that jet inlets that are known to have nonsymmetrically shedding initial boundary layers, namely those from the orifice or long pipe, cause jet precession to be induced more easily than the smooth contraction inlet, which is known to have a symmetrically shedding initial boundary layer. The nature of the exit flow is dominated by the degree to which a given configuration generates precession. Nevertheless, the three different inlet conditions also produce subtle differences in the exit profiles of mean velocity and turbulence intensity when the flow does precess reliably.

C.Y. Wong (✉), G.J. Nathan
Mechanical Engineering Department,
University of Adelaide,
North Terrace, 5005 Adelaide, South Australia
E-mail: cwong@mecheng.adelaide.edu.au
Fax: +618-83034367

T. O'Doherty
School of Engineering,
Division of Mechanical Engineering,
University of Wales, Cardiff, Wales, CF24 0YF, UK

Roman symbols

d	diameter of inlet (m)
D_1	diameter of FPJ chamber (m)
D_2	diameter of FPJ chamber exit lip (m)
E	expansion ratio D_1/d
f	frequency (Hz)
f_p	precession frequency (Hz)
h	step height $(D_1$-$d)/2$ (m)
n	power law index to describe pipe inlet jet (dimensionless) or nth sample passing through LDA probe volume
N	total number of bursts sampled (dimensionless)
r	radial distance from FPJ chamber axis (m)
rms	root-mean-square or fluctuating velocity component, $\sqrt{\overline{u^2}}$ (m/s)
R_1	radius of FPJ chamber (m)
R_2	radius of exit lip (m)
Re	Reynolds number $u_i d/v$ (dimensionless)
$S(f)$	arbitrary power spectrum (m²/s)
St	Strouhal number, $f_p h/u_i$ (dimensionless)
Δt_n	residence (or transit) time of a particle moving through the LDA probe volume (s)
u	axial component of mean velocity (m/s)
u_{cl}	axial component of mean centreline velocity (m/s)
u_i	bulk inlet velocity near the inlet plane (m/s)
u_n	velocity of the nth particle through the LDA probe volume (m/s)
u_{vc}	axial component of mean velocity in the region of the vena contracta (m/s)
u'	axial component of rms velocity (m/s)
v	radial component of mean velocity (m/s)
v'	radial component of rms velocity (m/s)
w	tangential component of mean velocity (m/s)
w'	tangential component of rms velocity (m/s)
x	axial distance from FPJ chamber inlet plane (m)
x'	axial distance from FPJ chamber exit plane (m)

Greek symbols

v	kinematic viscosity of air at 21°C, 14.7×10⁻⁶ m²/s

1
Introduction

The fluidic precessing jet (FPJ) nozzle shown in Fig. 1 has found application as a burner for rotary cement and lime kilns. Use of the FPJ burner gives a significant reduction in emissions of oxides of nitrogen (NO_x) relative to

conventional burners, some fuel savings and an improvement in product quality (Manias and Nathan 1994; Manias et al. 1996). Since its discovery (Nathan 1988) and subsequent patent (Luxton et al. 1991), much research has been invested to study the behaviour of this naturally oscillating jet flow. Research in the last decade has focused on the external mixing field of a wide range of precessing jet nozzles, including those that closely resembled the industrial configurations. Measurements on such configurations were performed under isothermal (Parham 2000) and combustion (Newbold et al. 2000) conditions.

In its simplest form, the FPJ nozzle is a cylindrical chamber with a small axisymmetric inlet at one end and an exit lip at the other (Fig. 1). The inlet flow separates at the inlet and reattaches asymmetrically to the wall of the chamber. A rotating pressure field is established within the chamber, which causes the reattaching flow to precess around the inside wall of the chamber; this also produces a precessing exit flow (Nathan et al. 1998). Here, the internal or external precession refers to the oscillatory motion of the developing jet about the geometric axis of the FPJ nozzle, as shown in Fig. 1, by the thick arrows either labeled "internal precession" or "external precession", respectively.

The flow within the nozzle is also bistable and switches intermittently between the precessing jet (PJ) mode, described earlier, and an axial jet (AJ) mode (Nathan et al. 1998). The flow in the AJ mode does not exhibit the asymmetric reattachment or the dominant precessing motion associated with the PJ mode. Instead, the local jet is located predominantly on the nozzle axis. The proportion of time spent in each mode depends on the nozzle geometry and Reynolds number (Nathan et al. 1998).

In the PJ mode, the interaction of the reverse induced air flow with the emerging external jet near the end of the chamber results in the formation of a transverse pressure gradient at the exit plane. This causes the exiting flow to deflect across the face of the nozzle outlet (Fig. 1). Deflection of the emerging precessing jet is further enhanced through the placement of an exit lip at the exit plane. The flow emerging from the exit plane is highly three-dimensional and unsteady, with both the exit angle and precession frequency exhibiting considerable cycle-to-cycle fluctuations. These issues combine to render measurements difficult.
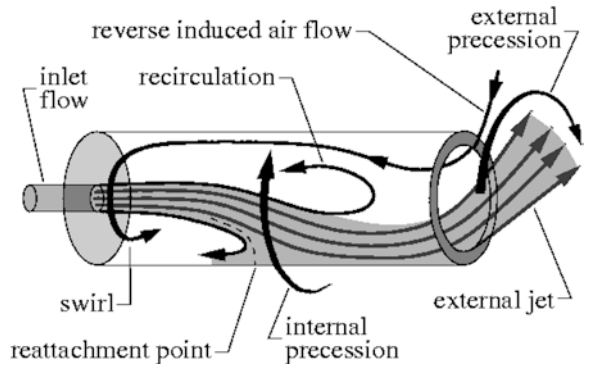

Fig. 1. Simplified representation of the flow in a fluidic precessing jet nozzle inferred from flow visualization

Various inlet flows to the nozzle have been used previously. These included a uniform velocity distribution produced by a contoured nozzle inlet, the flow emerging from a long pipe and the flow produced by a sharp-edged orifice plate, which is known to form a vena contracta just downstream from the sharp edge. Nathan (1988), using flow visualisation, showed that each of these inlet flows could produce jet precession and deduced that the presence or absence of precession dominated the characteristics of the exit flow. However, he did not investigate these effects in detail and did not quantify the exit velocity.

Mi et al. (2001), employing nie-sattering showed that in an unconfined jet the three initial conditions mentioned earlier produce significantly different near-field turbulent flow structures, and that these differences propagate into the far field. They observed that the contoured nozzle produces relatively large and fairly symmetric roll-up structures in the near field. In contrast, the pipe jet produces less evidence of large-scale organised motions, although smaller roll-ups were observed to be "randomly" formed around the jet periphery. The sharp-edged orifice plate also generated distinct, roll-up structures, which tended to be shed asymmetrically. The structures shed from the orifice plate were observed to be somewhat smaller than the structures generated by the contraction. Mi et al. (2001) reasoned that the increased asymmetry could be due to the strong upstream separation and recirculation regions that are present for the orifice plate but not for the other nozzles. The deductions by Mi et al. (2001) were observed using concentration measurements. Further support for these deductions is found in the recent PIV measurements of Wong et al. (2003c), who presented near-field vorticity images for each of these three jets. Other authors, such as Reeder and Samimy (1996) and Zaman (1999) used small tabs at the edge of a contoured nozzle to generate an initially asymmetric shear layer. They found that such tabs increase the rates of jet mixing and entrainment substantially.

Quinn (1990) examined the flow of a free jet from an asymmetric (triangular orifice) inlet and found that its Reynolds shear stress levels were higher than that from a smooth contraction inlet. He reasoned that the higher shear stress levels promoted mixing. Recently, Lee et al. (2001) used a triangular orifice for an inlet condition expanding suddenly into a short chamber, somewhat analogous to the present FPJ nozzle. Their flow visualisation experiments concluded that the asymmetric (triangular) jet inlet also generated a dominant oscillation of the jet, similar to the jet precession described earlier. However, jet oscillation in their case occurs for a larger equivalent diameter over a wider range of Reynolds numbers and configurations than is possible for the FPJ configurations presented. They deduced that the increased asymmetry within the inlet jet was a contributing factor in promoting this dominant oscillation.

These issues provide the motivation for the present investigation. This paper seeks to quantify the effect of circular inlet conditions produced by a long pipe, a contoured nozzle and an orifice plate on the resulting precessing jet flow in terms of axial, radial and tangential velocities and frequency of precession for each of three

different nozzle configurations. This knowledge is useful for nozzle design engineers and serves as a platform for future research involving the use of various inlet conditions.

2
Experimental details

The study assessed three inlet conditions for each of three nozzle configurations shown schematically in Table 1 along with the notation. The notation is obtained by combining the labels in the abscissa and ordinate. For example, the notation Pipe (Ch, L, CB) refers to the top right case with the pipe inlet connected to a chamber with a lip and centrebody.

2.1
Air supply and seeding

Laser-Doppler anemometry (LDA) measurements were conducted at the Mechanical Engineering Department at the University of Wales, Cardiff. A laboratory compressor with a capacity of 4000 l/min at 600 KPa supplied air to the experimental nozzles used in the experiment. The compressed air was passed through a 2000 l/min flow meter and then directed to a seed ejector. The seed ejector entrained sub-micron "HAZE" glycol particles produced by an external fog generator (ROSCO 4500). Each of these particles had a nominal diameter of less than 1 μm and a density ratio relative to air of 800. The frequency response of a typical particle was 7.35 kHz. This value was estimated using an approximate equation derived from Stokes' equation following Melling and Whitelaw (1975) and Durst et al. (1981). At this frequency, the ratio of the amplitude of such a particle's oscillation to the amplitude of surrounding fluid oscillation was greater than 0.99. This means that the particles were sufficiently small to follow the bulk flow with negligible time lag. The outlet from the seed ejector was connected to a long flexible hose. This, in turn, was coupled to either a long pipe or a flow conditioner for the smooth contraction and orifice inlets. Part of the fog was divided to seed the entrained ambient flow so that there was seeding of both the surrounding ambient and jet fluids. This was to minimise a bias towards higher velocities that would occur if only the jet flow was to be seeded (Durst et al. 1981). The experimental arrangement is shown schematically in Fig. 2. The present arrangement did not allow the flow meter to directly measure the total flow rate through the nozzle and resulted in different Reynolds numbers being used for each inlet condition tested. However, the actual flow through each inlet was quantified separately by integrating mean velocity profiles measured 1d from the nozzle inlet plane. These values are summarised in Table 2.

2.2
Flow conditioner

To remove residual upstream swirl, to reduce the turbulence intensity level of the flow and to make the flow at the inlet uniform, the current investigation adopted a flow-conditioning system based on the recommendations of Bradshaw and Pankhurst (1964). Flow conditioning was first achieved by a development pipe of 30 diameters in length connected in series with a conical diffuser with a total cone angle of 9.1° and an area expansion ratio of 2.1. This was followed by a honeycomb section with a length-to-diameter ratio of 12 to reduce any upstream swirl. A series of five screens, each with an open area ratio of 61% and screen wire diameter of 0.355 mm was used to further improve the flow uniformity and to reduce the turbulence intensity of the flow. A development section equivalent to about 280 wire diameters followed immediately after the last screen to allow any vortical structures generated by the screens to dissipate. Further details can be obtained from Wong et al. (2003a).

To obtain a uniform velocity profile at the FPJ inlet plane, a nozzle with a fifth-order polynomial profile with zero derivative end conditions and a contraction area ratio of 10.03 was attached to the end of the development section. Alternatively, a 5-mm thick sharp-edged orifice plate with a downstream chamfer of 45° was attached to the end of the development section. This type of flow normally results in the formation of a thin waist (vena contracta) just downstream from the sharp edge.

To obtain a pipe flow inlet, an upstream development length of about 95 pipe diameters following a honeycomb

Table 1. Schematic diagrams of the nine configurations of precessing jet nozzles examined in the experiment along with the symbols and notations which are used throughout the paper
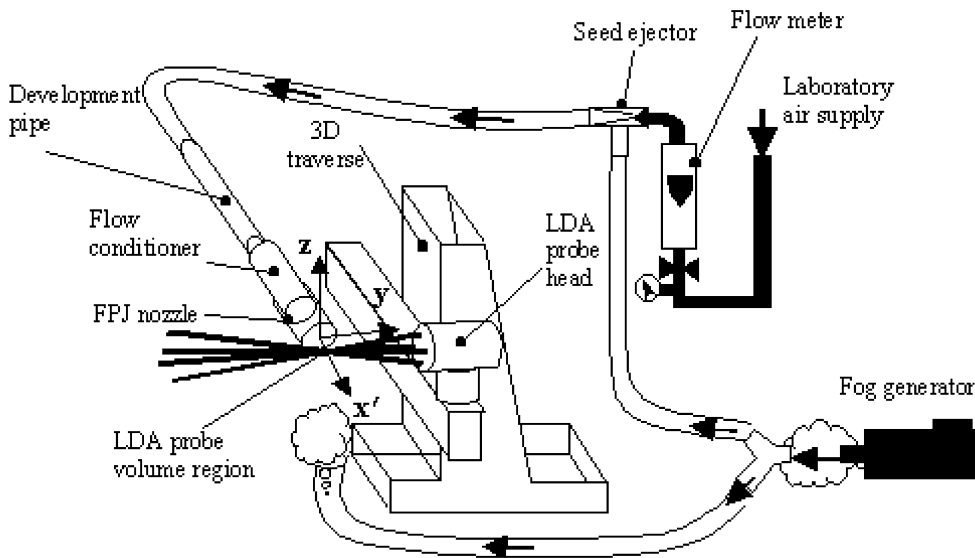
Fig. 2. Schematic diagram of the experimental arrangement. For clarity, the light generation system, burst spectrum analysers and the support for the flow conditioner are not shown

Table 2. Summary of inlet conditions used for the FPJ nozzles

Type of inlet	Bulk velocity $u_i(m/s)$	Reynolds number based on d and u_i (measured at $x/d=1$)
Pipe	103	111,000
Contraction	140	150,000
Orifice	96	103,000

flow straightener was used instead of the flow conditioner. This is substantially longer than the minimum of 40 diameters suggested by Hinze (1975) to be necessary for ensuring a fully developed turbulent flow in a pipe. All the inlet diameters d were kept the same at 15.79 mm.

2.3
Laser-Doppler anemometer
The two-component laser-Doppler anemometer used the 514.5 nm (green) and 488.0 nm (blue) lines from a 5-W argon-ion laser (Coherent Innova 70). Each line was split, with one beam from each pair frequency shifted by 40 MHz using a Bragg cell to remove directional ambiguity. Clock-induced bias caused by the frequency shift was corrected following Graham et al. (1989). A fibre-optic system for collection in backscatter mode was used for delivery and collection for a beam spacing of 64 mm and a lens focal length of 310 mm. The ellipsoidal probe volume had a length of 1.65 mm and a nominal waist diameter of 0.170 mm for the green beam and 1.57 mm by 0.162 mm for the blue beam. The average probe length was about 2% of the FPJ nozzle diameter D_1. This probe was traversed by a three-axis traverse system (Dantec) with a positional accuracy of 0.05 mm in three orthogonal directions. One axis of the traverse was aligned parallel to the axis of the nozzle (Fig. 2). Time-averaged measurements were performed in burst mode, while the burst spectrum analysers (BSA) were programmed to collect up to 10,000 velocity samples. The time-out for each incoming data record was set at 200 s.

2.4
Procedure and data correction scheme
The measurements of the flow through the FPJ nozzle were all performed with an inlet Reynolds number (based on inlet throat diameter d and bulk velocity u_i) of greater than 100,000 (Table 2). The LDA probe volume was positioned at $x'/d=0.63$ downstream from the nozzle exit plane (Fig. 3). Measurements were performed at 46 locations equally spaced at 2 mm along a radial line across the entire exit plane for all 9 configurations (Table 1). When measuring the axial component of velocity u, the blue beam pair was used. The green beam pair was used to measure the radial v and tangential w velocity components. The green beam pair had a higher energy distribution than the blue beam pair and was better at resolving the motion of weakly scattered seed particles usually moving in a direction perpendicular to the bulk flow (i.e., the tangential and radial components). In measuring the axial and radial components, the probe was traversed along the y-axis. Similarly, to acquire the axial and tangential components, the probe was moved along the z-axis.

It is well known that during velocity measurements of turbulent flows using LDA, a source of systematic error is introduced into the accuracy of the mean values. McLaughlin and Tiederman (1973) reported that direct arithmetic averaging of the LDA data often overestimates the actual mean velocity. This is because a disproportionate number of measurements are recorded during periods of high velocities since more particles pass through the volume in a given time. They suggested a one-dimensional correction scheme based on weighting each sample by a weighting factor inversely proportional to the measured velocity component of the nth sample u_n. However, their correction scheme was best applied to steady one-dimensional flows in which the local turbulence intensity, $u'/u\times100$, is not greater than 15% (Buchhave et al. 1979). McLaughlin and Tiederman (1973) concluded that for turbulence intensities up to 35%, an accuracy of 2 to 3% can be achieved. However, such a correction is not applicable to the present flow, which is highly three-dimensional and where local turbulent intensities of around 100% are
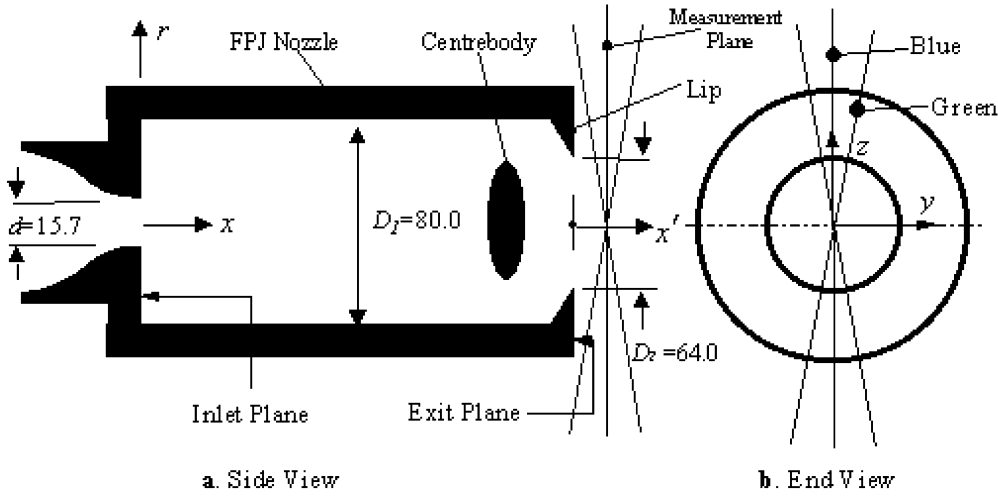
Fig. 3a,b. The coordinates and dimensions of the FPJ nozzle: **a** Side view. **b** End view. Mean velocities in x (or x' for the flow beyond the exit plane), z and y directions are represented as u, v and w, respectively, in the text and graphs. Root mean-squared (rms) values are similarly represented as u', v' and w', respectively. All dimensions in millimeters

not uncommon (by inspection of Figs. 6, 7 and 8). For such a flow measured using LDA processors in burst mode, Buchhave et al. (1979) suggested the method of transit-time weighting. The transit-time weighting method of correction was applied to all the velocity data reported in the present investigation and involved the averaging of velocities for those periods (transit or residence times) where there were LDA burst signals. The general equation used in the calculation of the transit-time weighted mean velocity was

$$u = \frac{\sum_{1}^{N} u(t_n)\Delta t_n}{\sum_{1}^{N} \Delta t_n}, \tag{1}$$

where $u(t_n)$ referred to the nth realisation of velocity, Δt_n referred to the transit time of a particle moving through the LDA probe volume and N referred to the total number of bursts sampled. The fluctuating velocity term was calculated in a similar fashion as

$$u' = \frac{\sum_{1}^{N} [u(t_n) - u]^2 \Delta t_n}{\sum_{1}^{N} \Delta t_n}. \tag{2}$$

In the present results, the ratio of transit-time weighted mean velocity results to uncorrected mean data is typically 0.75, while the corresponding ratio for the rms velocity results was approximately 0.90. In the region $-0.85 < \left(\frac{r}{R_1} \text{ or } \frac{r}{R_2}\right) < 0.85$, where adequate seeding exists and where sampling rates are high, the typical random error for a 95% confidence interval is approximately ±3%. Finally, the correctly weighted velocities were normalized by the transit-time weighted bulk velocity u_i from the respective inlet flows, which are summarised in Table 2.

3
Results and discussion

3.1
Inlet flow description
Preliminary velocity distributions were measured for three inlet conditions to check for flow symmetry. These

measurements were conducted in a free environment with the FPJ chamber removed. This avoided the optical distortion associated with the chamber and allowed comparison with other investigations. In general, the radial distributions of the mean axial velocities for the three inlets are symmetric and match published data well as shown by the results in Figs. 4 and 5. Further details of

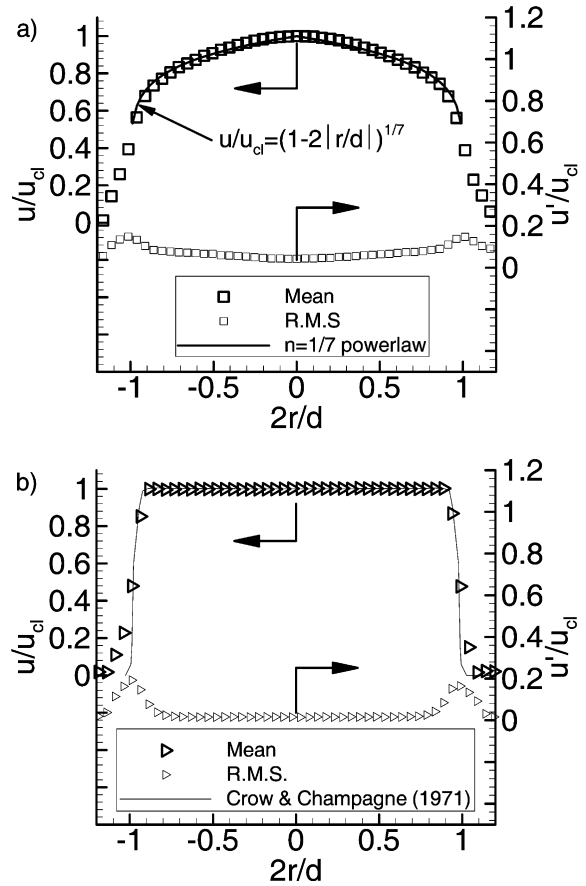Fig. 4a, b. Axial mean u and rms u' velocity distributions of: **a** Pipe jet obtained at x/d=0.34 (u_{cl}=41.5m/s). **b** Contraction jet obtained at x/d=0.56 (u_{cl}=40.5m/s). All values are normalised with the centreline velocity u_{cl}. Crow and Champagne (1971) data were obtained at x/d=0.025 for Re=83,000, and $u'/u_{cl} \times 100$ were 0.5% (on the centreline) and 8% (at the shear layer)
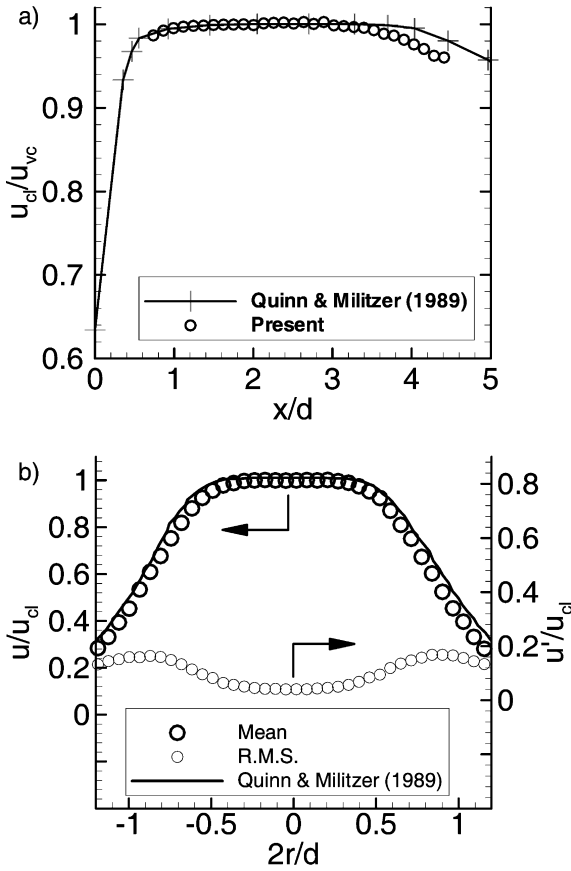
Fig. 5. a Mean axial velocity along the centreline for the present orifice (O) jet compared with literature data. **b** Axial mean u and rms u' velocity distribution with values normalised to centreline velocity u_{cl}=50.8m/s. Measurements taken at x/d=2.60 for Re=56,900. Quinn and Militzer (1989) measured at x/d=2.67 for Re=208,000 and their $100u'/u_{cl}$ were 4.7% (on the centreline) and 15% (at the shear layer) respectively. Here u_{vc} is the mean velocity in the region of the vena contracta near to x/d=2.60

these preliminary inlet measurements are summarised in Table 3.

3.2
FPJ exit plane results

The exit flows are presented in Fig. 6 for the Chamber configuration, in Fig. 7 for the chamber and lip configuration, and in Fig. 8 for the chamber, lip and centrebody configuration. All velocities are normalised relative to the bulk mean inlet velocity u_i. This accounts for the differences in throughput for the various inlets (Sect. 2.1), while allowing the differences in velocities through the nozzle to be compared, which would not have been possible if the data were normalised by the mean exit value. The characteristic differences associated with each general

nozzle configuration are considered first. Subsequent sections address the differences associated with each inlet. Note also that the values on the abscissa for Fig. 6 were normalised by the chamber radius R_1, while those for Figs. 7 and 8 were normalised by the exit lip radius R_2. This allows the effect of exit geometry on the velocity field to be assessed more easily.

The contraction (Ch) in Fig. 6a (mean) produces a mean exit axial velocity profile with a characteristic bell shape. For the chamber and lip, shown in Fig. 7a (mean), two of the three mean exit profiles are quite different, with a double peak showing the jet emerging from the outside of the nozzle. With the centrebody included, the double peak in the mean profile is very consistent and occurs for all inlet types (Fig. 8a, mean). These differences can be explained by the dynamics of the flow investigated previously. As discussed earlier, the flow in the chamber is known to be bimodal and can switch between an axial jet (AJ) and a precessing jet (PJ) mode (Nathan et al. 1998). The presence of an exit lip greatly favours the precessing mode over the axial mode. The "bell shape" in the mean profiles of the present measurement can therefore be associated with the AJ mode. By similar reasoning, the double-peak profile can be associated with the PJ mode. Figure 1 illustrates that the instantaneous jet in the PJ mode emerges from only one "side" of the chamber. This is similar to the phase-mean distribution of the axial velocity component quantified by Wong et al. (2003a), where the peak is shown to be on one side of the axis. When data are randomly taken over some time during the PJ mode, a double peak in the time-mean velocity profile is obtained, as was shown earlier by the total pressure measurements of Nathan (1988).

When interpreting the radial results, it should be noted that an outward flow from the nozzle axis corresponds to $v<0$ for $r>0$ or $v>0$ for $r<0$, and vice versa for inward flow. The radial distributions of the axial rms velocity also exhibit a strong dependence on the flow mode. Those cases corresponding to the AJ mode also exhibit a bell-shaped radial rms velocity profile (Fig. 6b, RMS). In contrast, the flow in the PJ mode exhibits the side peaks in the radial rms profile corresponding to the edge of the nozzle (Fig. 8b RMS). A higher rms in the side peaks would be expected with the oscillating motion associated with the emerging precessing flow (Nathan et al. 1998 and Wong et al. 2002).

The magnitudes of both the peak axial (u'/u) and radial turbulence intensity (v'/u), by inspection of Figs. 7 to 8, are generally greater than 100% in the PJ mode; these are also consistent with the dominance of the precessing motion. (Note that the rms values in Figs. 6 (RMS) to 8

Table 3. Conditions at which velocity distributions of the respective inlets were obtained

Type of inlet	Bulk velocity u_i (m/s)	Reynolds number $\frac{u_i d}{\nu}$	Turbulence intensity at the jet centreline $u'/u_{cl} \times 100$ (%)	Turbulence intensity at the jet shear layer $u'/u_{cl} \times 100$ (%)	Measurement distance from the inlet plane
Pipe	36.6	39,300	4.2	15	0.34d
Contraction	40.1	43,100	1.8	18	0.56d
Orifice	53.0	56,900	4.1	17	2.60d

(RMS.) are normalised by the bulk inlet velocity u_i, which is nominally ten times the mean exit velocity.)

3.2.1
The effect of initial conditions on the chamber configuration

Figure 6 presents the mean and rms velocities at the exit plane for the chamber only configuration, i.e. without the lip or the centrebody. Examining the mean axial components in Fig. 6a (mean), it is clear that the orifice and pipe inlets exhibit significantly different behaviour from the smooth contraction. Where the latter has the distinct bell-shaped profile associated with the AJ mode, the orifice and pipe inlets exhibit both considerably more scatter and have two dominant side peaks superimposed on a central peak. This is consistent with the flow switching intermittently between the two modes discussed earlier. Since the measurements were not conditioned upon the mode, different points will be measured with different proportions of AJ and PJ mode. Thus, where a profile may contain both the central and side peaks, some points were measured with the flow more in one mode than the other. This is responsible for the scatter, notably for the orifice and pipe inlets in Fig. 6a (mean) and for the lack of symmetry in the radial (Fig. 6b mean) and tangential (Fig. 6c mean) profiles. The higher axial rms velocities in the orifice and pipe data are also consistent with mode switching as shown in Fig. 6a (RMS). Together, these data suggest that the orifice and pipe inlets are more conducive to generating the PJ mode than the smooth contraction case in the chamber only configuration.

The radial mean profiles shown in Fig. 6b (mean) exhibit considerable scatter caused by mode switching. The trends associated with the PJ mode are clear in Fig. 8a (mean) and are therefore discussed in Sect. 3.2.3. However, it is evident that the trends in the radial mean velocities for the orifice and pipe inlets are relatively similar, with values close to zero on average, and show considerable scatter. In contrast, the smooth contraction inlet produces results with a greater mean radial velocity.

Fig. 6a–c. Time-averaged mean (u,v,w) and rms (u',v',w') velocity profiles for chamber-only case: **a** Axial. **b** Radial. **c** Tangential. All velocity values are normalised with the respective bulk inlet velocity u_i for each inlet case. The abscissa is normalised with the chamber radius R_1. The origins of the upwards-shifted ordinates are indicated on the right axis for contraction (*right-facing triangles*) and orifice (*circles*) inlets, respectively. The left axis refers to the pipe case (*square symbols*). *Symbols* as per Table 1
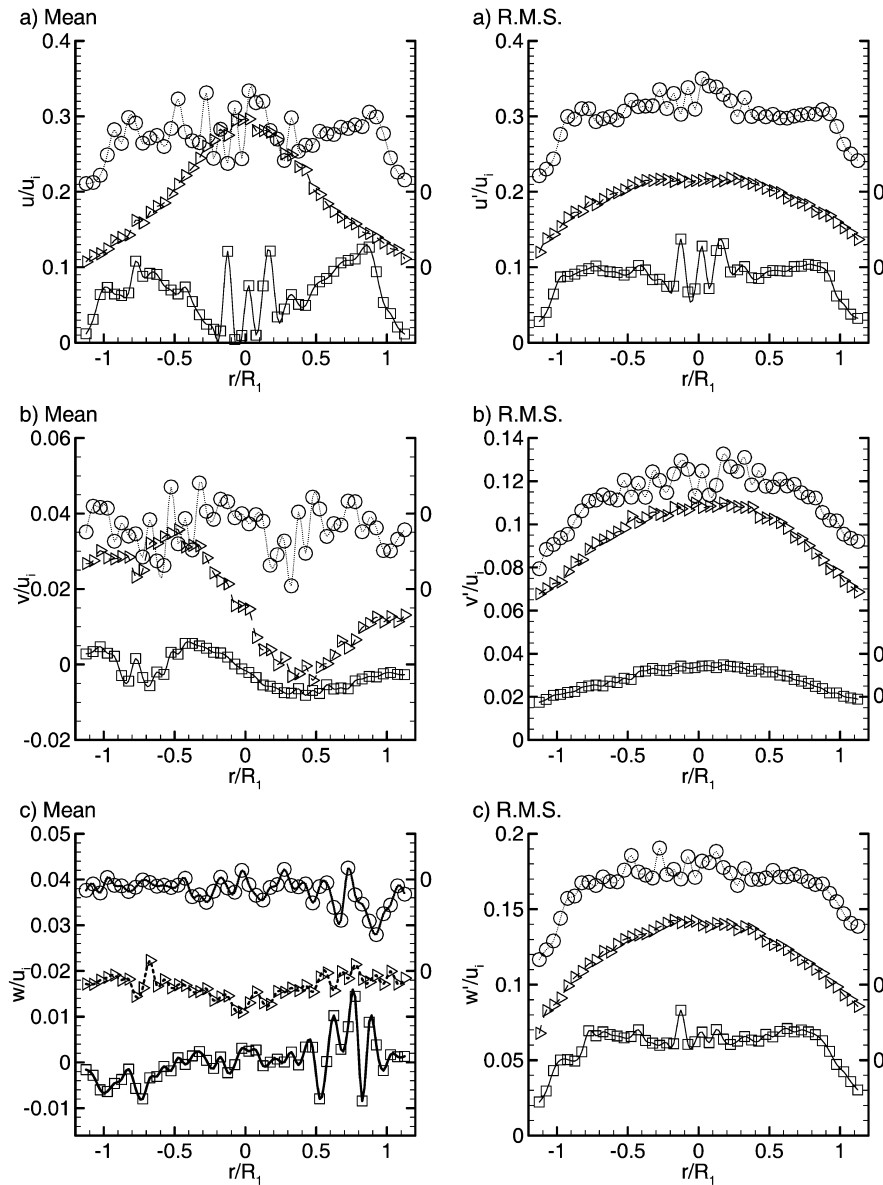
Fig. 7a–c. Time-averaged mean (*u*,*v*,*w*) and rms (*u'*,*v'*,*w'*) velocity profiles for chamber and lip case: **a** Axial **b** Radial. **c** Tangential. All velocity values are normalised with the respective bulk inlet velocity u_i for each inlet case. The abscissa is normalised with the exit lip radius R_2. The origins of the upwards-shifted ordinates are indicated on the right axis for contraction (*right-facing triangles*) and orifice (*circles*) inlets, respectively. The left axis refers to the pipe case (*square symbols*). *Symbols* as per Table 1
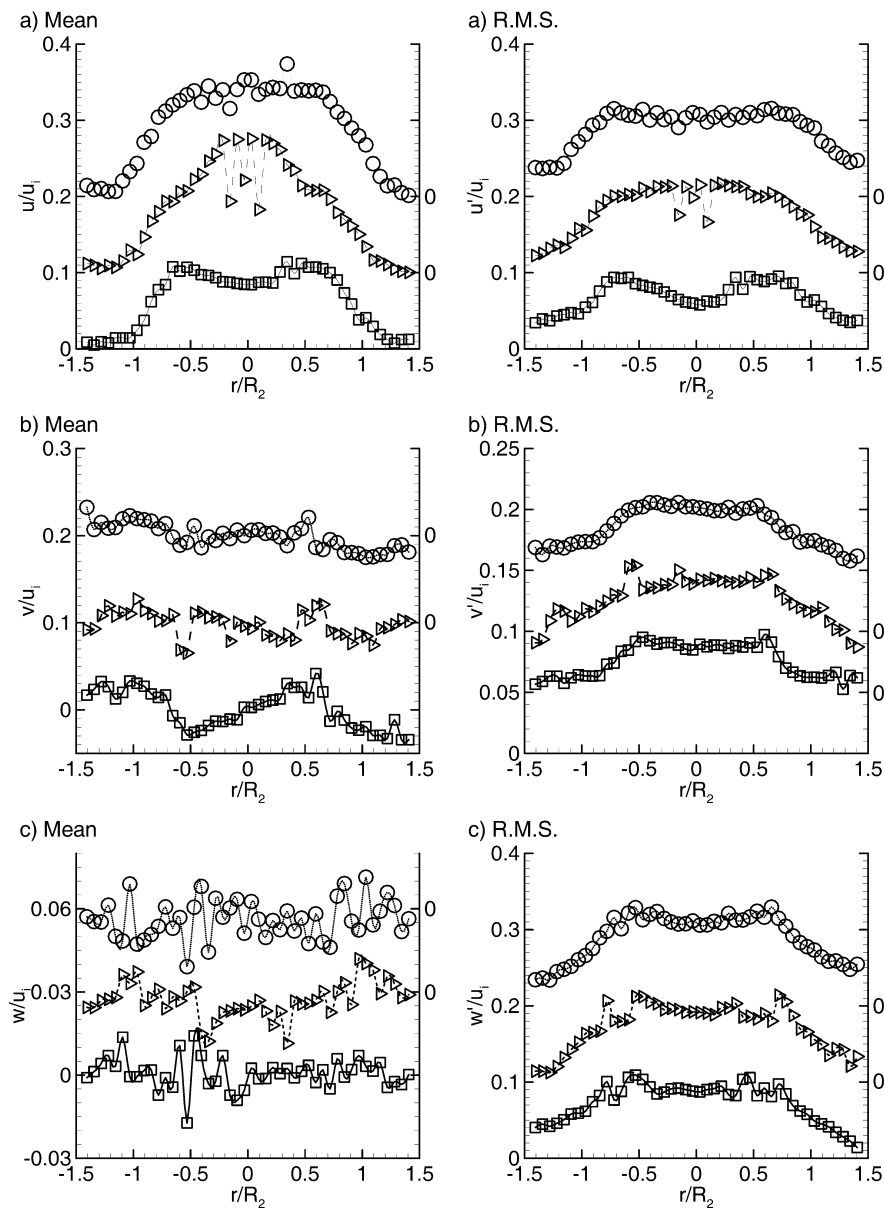
The trends in the rms velocities are different, with the pipe inlet having a much lower radial rms velocity than the other two inlets. The magnitude of the radial rms of the pipe and orifice configurations are approximately three times the absolute mean values at $r/R_1=\pm0.5$. This is consistent with a large exit angle for the PJ flow mode (shown in Sect. 3.2.3). The high level of mode-switching results, on average, in a flow with low absolute radial mean velocity and high relative radial rms velocities at $r/R_1=\pm0.5$.

The data of the tangential mean profiles shown in Fig. 6c (mean) for all inlet types are scattered about zero and indicate that the flow in the chamber-only configuration does not have a preferred precession direction.

3.2.2
The effect of initial conditions on the chamber and lip configuration
Adding a lip to the chamber was found by Nathan et al. (1998) to promote the predominance of the PJ mode.

However, for the present measurements, there is still evidence of some influence of the AJ mode for all three inlets as shown in Fig. 7a (mean). Nevertheless, both Figs. 7a (mean) and 7a (RMS) show the presence of the side peaks associated with the PJ mode. These side peaks are more apparent for the pipe and orifice inlets compared with the contraction inlet. In addition, a typical frequency spectrum for the contraction (Ch, L) shown in Fig. 9 does not indicate a dominant frequency peak associated with the PJ mode. This further illustrates that a weaker PJ mode is associated with the contraction inlet compared to the other inlets.

The absolute magnitudes of the radial mean profiles in Fig. 7b (mean) are about twice those of the case without an exit lip (Fig. 6b mean). This suggests an increased dominance of the PJ mode for all the inlets when the exit lip is added. The general trend in the mean radial velocity follows the trends in Fig. 8b (mean) where PJ mode is prevalent. This further suggests that PJ mode is dominant for this type of configuration. The radial rms profiles in Fig. 7b (RMS) also indicate the dominance of the PJ mode
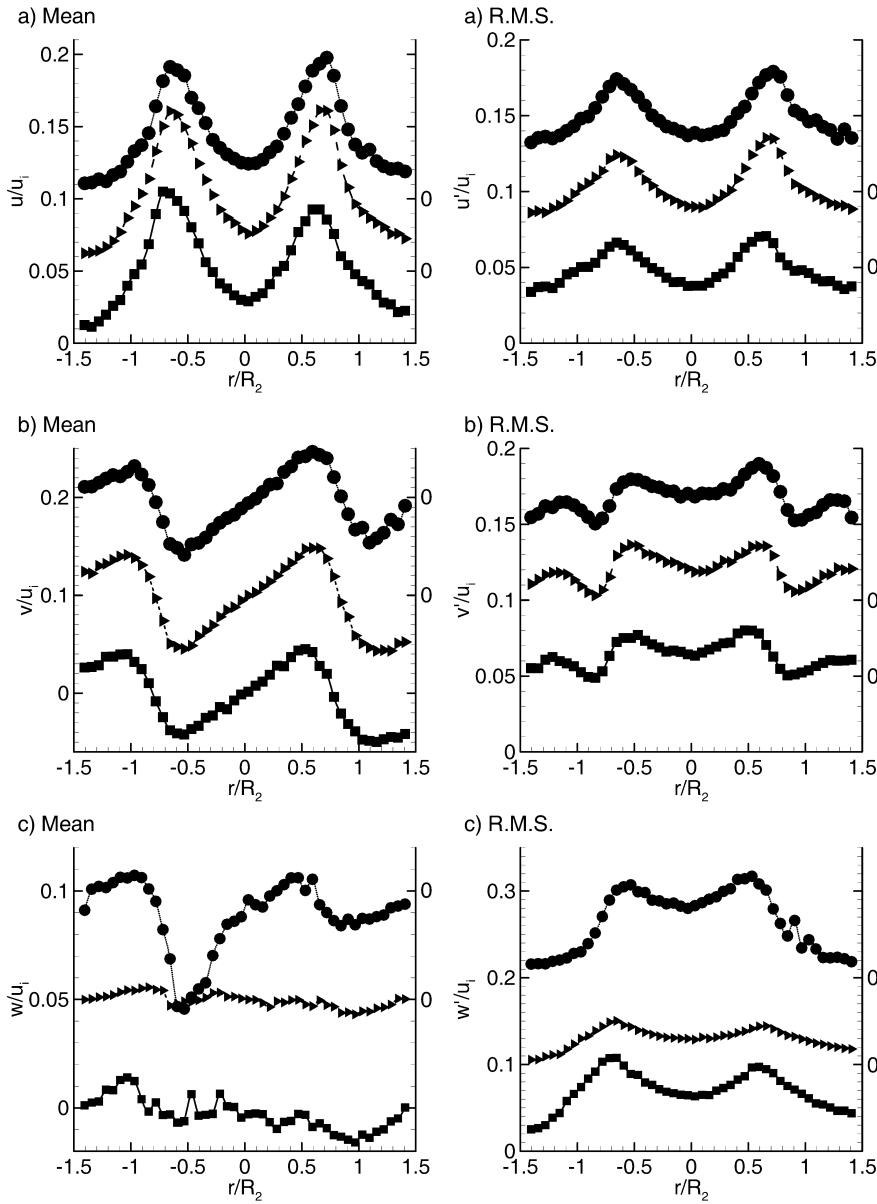
Fig. 8a–c. Time-averaged mean (u,v,w) and rms (u',v',w') velocity profiles for chamber, lip and centrebody case: **a** Axial. **b** Radial. **c** Tangential. All velocity values are normalised with the respective bulk inlet velocity u_i for each inlet case. The abscissa is normalised with the exit lip radius R_2. The origins of the upwards-shifted ordinates are indicated on the right axis for contraction (*right-facing triangles*) and orifice (*circles*) inlets, respectively. The left axis refers to the pipe case (*square symbols*). *Symbols* as per Table 1

through the high rms velocities for all three inlets. This is consistent with the dominance of the PJ mode resulting in the radial oscillation of the emerging precessing jet in these types of configurations.

The general scatter in the data of tangential mean velocities in Fig. 7c (mean) for all inlet cases indicates that the precessing jet again does not have a preferred precession direction. Nevertheless, the emerging jet does appear to have a strong tangential component since tangential rms profiles (Fig. 7c RMS) exhibit double peaks with about the same radial location and magnitude as the axial components.

3.2.3
The effect of initial conditions on the chamber, lip and centrebody configuration

The centrebody has a big influence on the flow field by stabilising the PJ mode. It almost eliminates the mode switching for all inlet conditions, as shown by the close collapse of the mean velocities in Figs. 8a and 8b especially. Nevertheless, the inlet flow also has a secondary influence on the emerging flow. The orifice inlet produces the highest exit rms and turbulence intensities for all three components, while the pipe produces the lowest (Fig. 8a). This is the same trend as occurs in a free jet (Mi et al. 2001), suggesting that these effects are superimposed on the now dominant precessing motions. The orifice inlet also results in the lowest peak axial velocity (Fig. 8a mean). This is consistent with the inlet jet having the greatest rate of local spread and decay in its path through the FPJ chamber, resulting in a lower peak exit velocity.

The radial velocity profile associated with the PJ mode is now clear (Fig. 8b mean). The peak and trough closest to the axis (indicating inward flow towards the axis) are slightly stronger than the outer peak and trough (indicating flow away from the axis). This is consistent with the local jet emerging from one side of the nozzle and being directed across the nozzle axis (Fig. 1). The weaker outer

peaks are associated with the spreading of the jet beyond the nozzle edge. These measurements are entirely consistent with recent PIV measurements by Wong et al. (2002), who showed that the time-averaged flow converges radially inward to a point approximately $0.5D_2$ downstream and then spreads rapidly outwards.

The introduction of the centrebody also appears to stabilise the direction of precession. This is evident from Fig. 8c (mean), in which a preferred mean tangential direction is shown for all the inlets. Interestingly, the locations of the inner peak and trough in the mean tangential profiles are coincident with the respective inner peaks and troughs in the axial and radial components. However, the locations of the outer peak and trough in the tangential mean component (Fig. 8c mean) are coincident with the weaker outer peak and trough in the radial mean component (Fig. 8b mean), consistent with ambient fluid being drawn eccentrically inward. This phenomenon was directly measured in a recent PIV experiment reported by Wong et al. (2003b). They demonstrated that the local (phase-averaged) precessing jet emerged with high radial and tangential components.

3.3
Frequency analysis of the various FPJ nozzles

The precession frequency f_P for each case is estimated from the axial velocity frequency spectrum obtained near $r/R_1=0.62$ or $r/R_2=0.78$ at a probe location used by Nathan et al. (1998) to detect jet precession. These measurements are presented in Fig. 9 as arbitrary energy spectra, in which the time-series velocity data have been resampled using linear interpolation with the maximum frequency determined by half the mean data rate.

In general, the chamber-only (Ch) configurations do not show distinct low-frequency peaks, but rather, a gradual "hump". This supports the earlier deductions that the AJ mode is dominant in this type of configuration. However, a slight peak near to 10 Hz for orifice (Ch) is consistent with the intermittent presence of the PJ mode as explained earlier in Sect. 3.2.1. All other configurations show distinct spectral peaks in the order of 10 Hz associated with jet precession (Nathan et al. 1998), except for the contraction (Ch, L) case in which only a weak peak associated with the PJ mode is observed near 30 Hz. These observations are consistent

Fig. 9. Typical log–log arbitrary spectral energy plots of the various configurations at $r/R_1=0.62$ or $r/R_2=0.78$ Notation as per Table 1. *Left column*: pipe inlet; *centre column*: contraction inlet; *right column*: orifice inlet
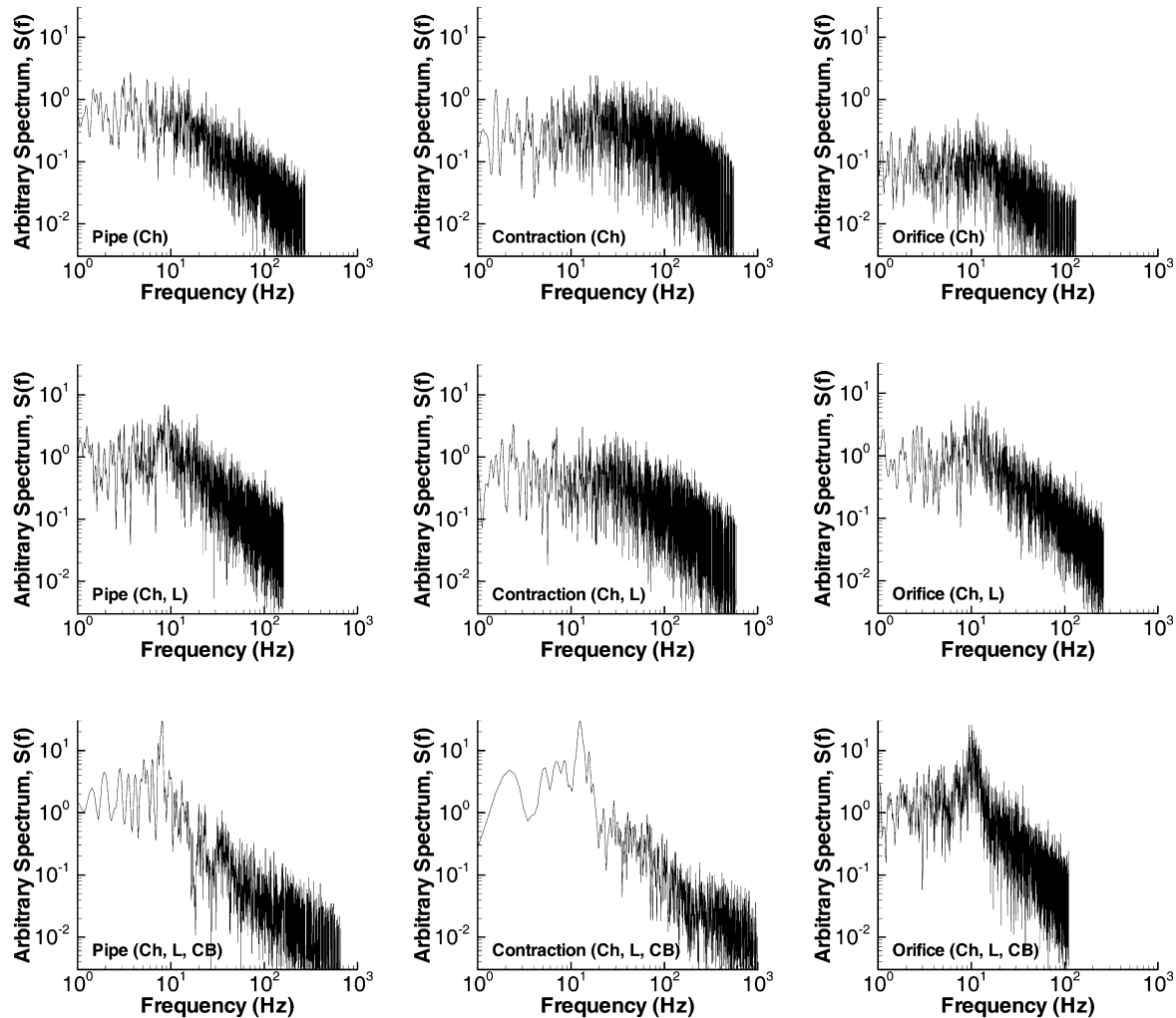
with the conclusions made earlier in Sect. 3.2.2 that the AJ mode generally dominates in the contraction (Ch, L) case.

A nondimensional Strouhal number St, was used to compare these precession frequencies with those in literature. Since not all configurations have a dominant precession frequency, as discussed above, only those configurations that do show distinct frequency peaks are presented, that is the Ch-L and Ch-L-CB configurations. The Strouhal number was calculated using Eq. (3), where $h=(D-d)/2$ and u_i is the bulk inlet velocity, following Nathan et al. (1998)

$$St = \frac{f_p \times h}{u_i}. \tag{3}$$

The Strouhal number was plotted against Reynolds number Re, defined by Eq. (4), where d=inlet diameter, and v=kinematic viscosity. The plot is shown in Fig. 10.

$$Re = \frac{u_i \times d}{v}. \tag{4}$$

The reliability of the present measurement is established by the excellent agreement of the present measurement of the orifice (Ch, L) configuration (E=5.0) with the comparable measurements by Nathan et al. (1998) with E=6.43.

The results, shown in Fig. 10, indicate that FPJ nozzles with the centrebody arrangement decrease St by approximately 10%, i.e. by 5×10^{-4}, in every case. The data also suggest that the initial conditions have a weak influence on St for Re>100,000, with the orifice having the highest St and the pipe the lowest. This trend suggests that increased spreading of the jet within the chamber acts to increase, albeit slightly, the frequency of precession. This idea is consistent with the deduction of Mi et al. (1999) that increasing the momentum of recirculated fluid within the chamber acts to increase the precession frequency. That deduction was based on the finding that frequency also increases with an increase in the chamber length for a fixed nozzle inlet. This agreement gives confidence that the measured trend is correct even though the data were measured at different Reynolds numbers.

4
Concluding remarks

The initial conditions of the jet entering the nozzle chamber contribute significantly to the flow within and emerging from an FPJ nozzle. Inlet conditions have a significant influence on the relative dominance of the precessing jet (PJ) or axial jet (AJ) mode. Those inlets that favour nonsymmetric shedding of the initial boundary layer and turbulent structures, namely the sharp-edged orifice plate and the pipe, cause jet precession to be induced more easily than the smooth contraction inlet, which is known to have a symmetrically shedding initial boundary layer. The notion regarding the asymmetry of shear layer shedding of the initial shear layer shedding is based on the findings made in the literature, especially of the experimental observations of Mi et al. (2001), who used a nie-sattering technique and of the recent PIV experiments of Wong et al. (2003c).

When the PJ mode is dominant, as occurs in the chamber–lip–centrebody configuration, the turbulence intensity is highest for the orifice inlet and lowest for the pipe inlet. Similarly, the peak mean axial exit velocity is lowest for the orifice inlet. These findings are also consistent with the trends in a free jet as noted by Mi et al. (2001), in which an orifice jet has the greatest rate of spread, decay and turbulence intensity, while the pipe jet has the lowest.

Likewise, the trend of the influence of initial conditions on the Strouhal number of precession is consistent with the trend in the spreading rate of free jets. That is, the precession Strouhal number of the jet from the orifice inlet is the highest, and that from the pipe is the lowest. However, these differences were shown to be relatively small. The present findings therefore suggest that the turbulence structure at the inlet is superimposed on the dominant precessing motion, and that this influence propagates to the nozzle outlet. This finding has a broader implication on other related types of complex flows, such as swirling flows in combustion chambers, boilers and furnaces, and generally where multiple inlet flows are superimposed on each other.

Although the present measurements have provided valuable quantitative data and insight into this complex and unsteady flow, they also highlight the limitations of time-averaged single-point measurements in obtaining instantaneous structural information regarding the FPJ flow. Planar techniques will allow these instantaneous structures to be identified and also assist in differentiating between various flow modes. At the time of writing, phase-averaged particle image velocimetry measurements in the near external field for the contraction (Ch, L, CB) case (Wong et al. 2003b) have been completed with the view to providing more detailed information into this complex and important flow.
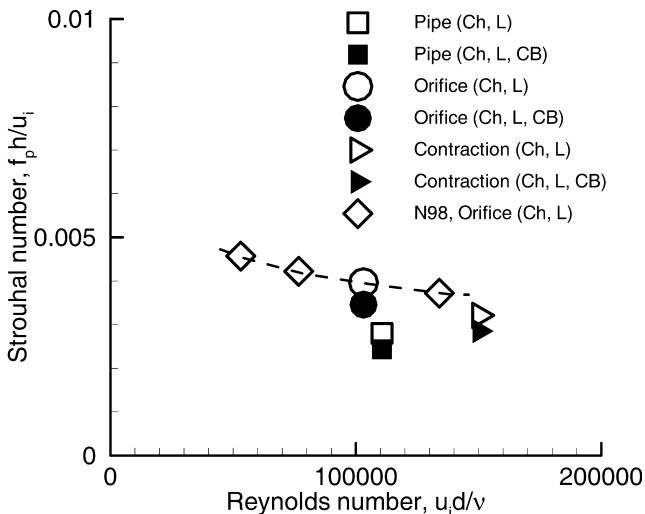

Fig. 10. Strouhal number versus Reynolds number plot of the various FPJ configurations compared with literature data. Note that results from chamber-only configurations are not shown since they do not show distinct frequency peaks. *N98* refers to the datum of Nathan et al. (1998)

References

Buchhave P, George WK Jr, Lumley JL (1979) The measurement of turbulence with the laser-Doppler anemometer. Ann Rev Fluid Mech 11:443–503

Bradshaw P, Pankhurst RC (1964) The design of low-speed wind tunnels. In: Kuchemann D, Sterne LHS (eds) Prog Aero Sci 5:1–69

Crow SC, Champagne FH (1971) Orderly structure in jet turbulence. J Fluid Mech 48:547–591

Durst F, Melling A, Whitelaw JH (1981) Principles and practice of laser-Doppler anemometry, 2nd edn. Academic, London

Graham LJW, Winter AR, Bremhorst K, Daniel BC (1989) Clock-induced bias errors in laser-Doppler counter processors. J Physics E 22:394–397

Hinze JO (1975) Turbulence, 2nd edn. McGraw-Hill, New York

Lee SK, Lanspeary PV, Nathan GJ, Kelso RM, Mi J (2001) Preliminary study of oscillating triangular jets. In: Dally BB (ed) Proc 14th Australasian fluid mechanics conference, Adelaide, Australia, 2:821–824

Luxton RE, Nathan GJ (1991) Controlling the motion of a fluid jet. US patent No. 5,060,867

Manias CG, Nathan GJ (1994) Low NO_x clinker production. World Cement 25:54–56

Manias CG, Balendra A, Retallack D (1996) New combustion technology for lime production. World Cement 27:34–39

Melling A, Whitelaw JH (1975) Optical and flow aspects of particles. In: Buchhave P. et al. (eds) Proceedings of the LDA symposium, Copenhagen, Denmark, pp 382–401

McLaughlin DK, Tiederman WG (1973) Biasing correction for individual realization of laser anemometer measurements in turbulent flows. Phys Fluids 16:2082–2088

Mi J, Nathan GJ, Nobes DS (2001) Mixing characteristics of axisymmetric free jets from a contoured nozzle, an orifice plate and a pipe. J Fluids Eng 123:878–883

Mi J, Nathan GJ, Hill SJ (1999) Frequency characteristics of a self-excite precessing jet nozzle. In: Proc 8th Asian congress of fluid mechanics, 6–10 Dec. International Academic Publishers, Shenzhen, China, pp 755–758

Nathan GJ (1988) The enhanced mixing burner. Dissertation, Department of Mechanical Engineering, University of Adelaide, Australia

Nathan GJ, Hill SJ, Luxton RE (1998) An axisymmetric 'fluidic' nozzle to generate jet precession. J Fluid Mech 370:347–380

Newbold GJR, Nathan GJ, Nobes DS, Turns SR (2000) Measurement and prediction of NO_x emissions from unconfined propane flames from turbulent-jet, bluff-body, swirl and precessing jet burners. In: Proc Combust Inst 28:481–487

Parham JJ (2000) Control and optimisation of mixing and combustion from a precessing jet nozzle. Dissertation, Department of Mechanical Engineering, University of Adelaide, Australia

Quinn WR, Militzer J (1989) Effects of nonparallel exit flow on round turbulent free jets. Int J Heat Fluid Flow 10:139–145

Quinn WR (1990) Mean flow and turbulence measurements in a triangular turbulent free jet. Int J Heat Fluid Flow 11:220–224

Reeder MF, Samimy M (1996) The evolution of a jet with vortex-generating tabs: real-time visualization and quantitative measurements. J Fluid Mech 311:73–118

Wong CY, Nathan GJ, Kelso RM (2002) Velocity measurements in the near-field of a fluidic precessing jet flow using PIV and LDA. In: McIntyre T (ed) Proc 3rd Australian conference on laser diagnostics in fluid mechanics and combustion, Brisbane, Australia, 2–3 Dec, pp 48–55

Wong CY, Lanspeary PV, Nathan GJ, Kelso RM, O'Doherty T (2003a) Phase averaged velocity in a fluidic precessing jet nozzle and in its near external field. J Exp Thermal Fluid Sci 27:515–524

Wong CY, Nathan GJ, Kelso RM (2003b) PIV of the unsteady flow emerging from a fluidic precessing jet nozzle using direction and phase triggers. In: Proc 7th Asian symposium on visualization, Singapore, 3–7 Nov, in press

Wong CY, Nathan GJ, Mi JC (2003c) The near-field structures of axisymmetric free jets from a contoured nozzle, a long pipe and an orifice plate (private communication)

Zaman KBM (1999) Spreading characteristics of compressible jets from nozzles of various geometries. J Fluid Mech 383:197–228